Frizzled3 is required for the development of multiple axon tracts in the mouse central nervous system

Zhong L. Hua[a], Sangmin Jeon[b,c,d,e], Michael J. Caterina[b,c,d,e], and Jeremy Nathans[a,c,f,g,1]

[a]Department of Molecular Biology and Genetics, [b]Department of Biological Chemistry, [c]Department of Neuroscience, [d]Department of Neurosurgery, [e]Neurosurgery Pain Research Institute, [f]Department of Ophthalmology, and [g]Howard Hughes Medical Institute, The Johns Hopkins University School of Medicine, Baltimore, MD 21205

Contributed by Jeremy Nathans, April 9, 2014 (sent for review February 15, 2014)

Targeted mutation of the *Frizzled3* (*Fz3*) gene in mice has been shown to disrupt the growth and guidance of a subset of peripheral and central axons. Here we used conditional deletion of *Fz3* to explore the forebrain territories in which *Fz3* action is required for the development of the anterior commissure and the corticothalamic, corticospinal, and thalamocortical tracts. Experiments with region-specific deletion of *Fz3* using a variety of Cre lines show that proper routing of corticothalamic and thalamocortical axons in the internal capsule requires *Fz3* expression in the ventral telencephalon. The pattern of defects among forebrain axon tracts that are induced by conditional deletion of *Fz3* conforms closely to the pattern previously observed with analogous conditional deletion of *Celsr3*, implying a close mechanistic link between Fz3 and Celsr3 in axon guidance. We further found that several central nervous system axon tracts require *Fz3* function as early as embryonic day 11.5, and that *Fz3* is required for pathfinding by dopaminergic and serotonergic axons in the brain and by a subset of optic tract axons. In addition, conditional deletion of *Fz3* in all tissues caudal to the neck eliminates the spinothalamic tract and the transmission of somatosensory information from the spinal cord to the brain, as determined by neuroanatomic tracing and behavioral testing.

planar cell polarity | Cre/loxP

Complexity within the mammalian nervous system can be roughly divided into two categories: cell type identity and morphology/connectivity. On its largest scale, the second category is exemplified by the many distinct patterns of long-range axonal trajectories within the adult CNS. The guidance mechanisms responsible for these axonal trajectories have been an object of longstanding interest to neurobiologists, and, over the past 20 y, a wide variety of attractive and repulsive axon guidance systems have been identified (1). For a few well-defined axon growth and guidance decisions—such as dorsal vs. ventral growth of limb motor axons and midline crossing of retinal ganglion cell (RGC) and spinal sensory axons—the roles of several guidance systems, including Slit/Robo, Ephrin/Eph, and Semaphorin/Plexin, have been intensively investigated (2, 3).

One recently discovered axon growth and guidance system uses some of the same molecular components that were identified in the context of epithelial polarity determination, a process referred to as tissue polarity or planar cell polarity (PCP). As first defined in *Drosophila*, PCP controls polarity within the plane of the epithelium and is mediated by a small number of integral membrane or membrane-associated proteins (4). Within the responsive epithelium, several PCP proteins are localized asymmetrically within each cell in a pattern that matches the large-scale vectorial asymmetry of the epithelium. In mice, two integral membrane PCP proteins, Frizzled3 (Fz3) and Celsr3, control a nearly identical set of axon growth and guidance processes, with loss-of-function mutations in either gene producing severe disruptions in the anterior commissure and the corticothalamic, thalamocortical, and nigrostriatal tracts (5–7). In the midgestation spinal cord, where the primary defect in $Fz3^{-/-}$ and $Celsr3^{-/-}$ axon development has been examined in detail, commissural sensory axons appear incapable of sensing the rostrocaudal vector after midline crossing (8). Recent work has revealed additional defects in $Fz3^{-/-}$ mice, including defective migration of a subset of neural crest cells, a failure of some cranial motor axons to reach their targets, and stalling of spinal motor axons that are destined to innervate the dorsal limb (9).

The present study addresses several open questions regarding the role of *Fz3* in CNS axon guidance. What is the effect of selectively deleting *Fz3* in the thalamus, cortex, striatum, retina, or spinal cord? What are the earliest defects in CNS axon guidance referable to loss of *Fz3*? Are there additional $Fz3^{-/-}$ axon growth/guidance phenotypes outside of the spinal cord that permit a distinction to be made between defective polarity and defective growth? Can selective disruption of particular axon tracts by regional deletion of *Fz3* be used to study the functional role of those pathways? We address these questions by visualizing defined axon tracts at early and late gestational ages and by deleting *Fz3* in selected CNS territories.

Results

Overview of Axon Tract Defects in the $Fz3^{-/-}$ Brain. As noted earlier, previous experiments demonstrated that *Fz3* is required for the development of several major axon tracts in the mouse forebrain (5, 6). These earlier experiments primarily used methods for visualizing axons, such as Neurofilament-M (NF) immunostaining, diffusion tensor MRI, and 1,1′-dioctadecyl-3,3,3′,3′-tetramethylindocarbocyanine perchlorate tracing, that identify axons based on their locations but do not distinguish among axons based on biochemical or other molecular properties of the cell of origin. In regions where axons from different tracts are closely apposed or interdigitated—as seen, for example, with the corticothalamic and thalamocortical tracts—these methods do not distinguish

Significance

Axons within the mammalian central nervous system must navigate with high accuracy over long distances. Tissue polarity (also called planar cell polarity) signaling is emerging as a major axon guidance system. *Frizzled3* (*Fz3*), a core polarity gene, is shown here to be essential for a wide variety of axon guidance decisions in the mouse brain and spinal cord beginning with the earliest axon trajectories in the day 12 embryo. In particular, this work shows that axon guidance defects in *Fz3* mutant embryos involve erroneous directions of growth rather than axon elongation per se. In adult mice in which the spinal cord is missing Fz3, anatomic and behavioral analyses show that sensory information from the limbs does not reach the brain.

Author contributions: Z.L.H. and J.N. designed research; Z.L.H. performed research; Z.L.H. and J.N. analyzed data; Z.L.H. and J.N. wrote the paper; and S.J. and M.J.C. supervised and assisted with mouse behavioral tests.

The authors declare no conflict of interest.

[1]To whom correspondence should be addressed. E-mail: jnathans@jhmi.edu.

This article contains supporting information online at www.pnas.org/lookup/suppl/doi:10.1073/pnas.1406399111/-/DCSupplemental.

the different classes of axons. To circumvent this limitation and obtain a more detailed and selective visualization of axon defects in $Fz3^{-/-}$ mice, we have supplemented these nonspecific methods of axon visualization with tract-specific methods, including Cre/loxP-based labeling of axons in a cell type- or region-specific manner, and immunostaining for the neurotransmitter-specific markers tyrosine hydroxylase (TH) and serotonin/5-hydroxytryptamine (5-HT) to visualize aminergic and serotonergic axons, respectively.

Fig. 1 compares the brain defects in $Fz3^{-/-}$ mice visualized by NF immunostaining with the trajectories of dorsal thalamic axons visualized with a *RORα-IRES-Cre* knock-in allele and a Cre-controlled human placental alkaline phosphatase (hPLAP; hereafter "AP") reporter, *R26iAP* (10, 11). In the prenatal mouse brain, *RORα* is expressed in the dorsal thalamus (12). As $Fz3^{-/-}$ mice die shortly after birth, we performed these analyses on WT ($Fz3^{+/-}$ or $Fz3^{+/+}$) and $Fz3^{-/-}$ brains at embryonic day (E) 18.5. The NF immunostaining shown in Fig. 1 *A*–*G*′ confirms and extends previous descriptions of the $Fz3^{-/-}$ brain phenotype (5, 6). In addition to the defects noted in the Introduction, the corticospinal tract was greatly reduced, the fasciculus retroflexus and the mammillothalamic tract were nearly completely absent, the medial lemniscus was less compact (Fig. 1 *E* and *E*′), and the regular matrix of axon bundles in the reticular formation was disorganized (Fig. 1 *F*–*G*′).

AP histochemical staining of *RORα-IRES-Cre*;*R26iAP*;$Fz3^{+/-}$ and *RORα-IRES-Cre*;*R26iAP*;$Fz3^{-/-}$ brain sections showed strong and selective labeling of thalamocortical neurons and axons (Fig. 1 *H*–*N*′). In the *RORα-IRES-Cre*;*R26iAP*;$Fz3^{-/-}$ brain, virtually none of the thalamic axons enters the striatum as they do in the WT control. Instead, most of the $Fz3^{-/-}$ thalamic axons project ventrally and then either create a novel tract along the floor of the midbrain to innervate the contralateral thalamus or project laterally for a short distance along the surface of the cortex. A small subset of the $Fz3^{-/-}$ thalamic axons project dorsally and posteriorly to the colliculus (Fig. 1 *M*′ and *Q*).

***Fz3* Is Required in Ventral Telencephalic Neurons for the Development of Corticothalamic, Corticospinal, and Thalamocortical Axons.** The major axon tracts in the mouse brain, including those affected by loss of *Fz3*, extend over long distances and are guided by extracellular attractive and repulsive cues, guidepost cells, and/or preexisting axons (13). *Fz3* is widely expressed in the developing mouse brain (6), but it is not known which of its expression domains is required for the growth and guidance of particular axon tracts. To address this question, we asked whether *Fz3* expression is required in cortical pyramidal, thalamic, or striatal neurons for the development of the anterior commissure, and the corticothalamic, thalamocortical, and corticospinal tracts. For these experiments, we combined a conditional *Fz3* allele ($Fz3^{CKO}$) (9) with transgene or knock-in alleles that express *Cre* in: (*i*) the dorsal thalamus (*RORα-IRES-Cre*) (10); (*ii*) the midbrain and hindbrain (*Dbx1-IRES-Cre*) (14); (*iii*) the dorsal telencephalon, including the neocortex (*Emx1-IRES-Cre*) (15); (*iv*) the ventral telencephalon, including a large region of the pallium (*Dlx5/6-Cre*) (16); and (*v*) the telencephalon but not the thalamus (*Foxg1-Cre*) (17). A detailed description of the topography of *Cre* action in several of these lines can be found in the work of Zhou et al. (18).

When *Fz3* was inactivated throughout the telencephalon (*Foxg1-Cre*;$Fz3^{CKO/-}$), the forebrain exhibited the full spectrum of axon defects seen in the $Fz3^{-/-}$ forebrain (Fig. 2 *B*–*B*″ and

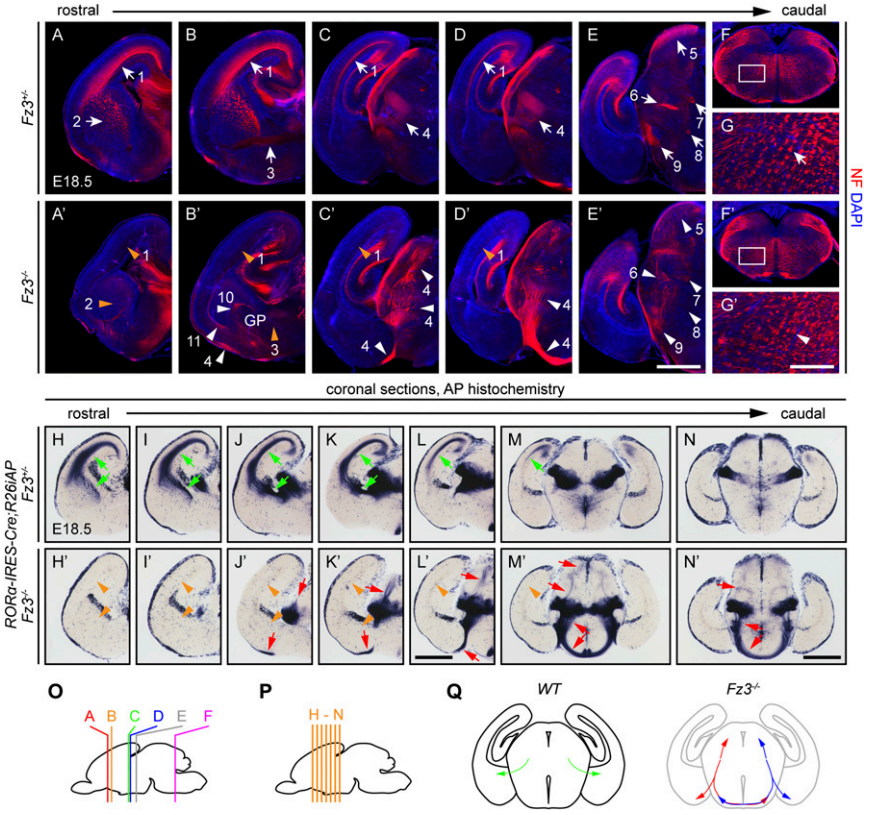

Fig. 1. In the brain, multiple axon tracts are affected by loss of *Fz3*. (*A*–*G*′) NF immunostaining of E18.5 coronal brain sections showing the normal position of axon tracts in the $Fz3^{+/-}$ brain (arrows) and aberrant (white arrowheads) or missing axon tracts (orange arrowheads) in the $Fz3^{-/-}$ brain. These include the absence of subcortical and striatal axons (*A* and *A*′); absence of the anterior commissure (*B* and *B*′); misrouting of thalamocortical axons (*C*–*D*′); a nearly complete absence of the corticospinal tract, the fasciculus retroflexus, and the mammillothalamic tract; and poor fasciculation of the medial lemniscus (*E* and *E*′). (*G* and *G*′) Enlarged views of boxed regions in *F* and *F*′, respectively, showing disorganization of reticular formation axons. Arrows and arrowheads designated by numbers point to different axons/tracts: (*1*) axons in the cortical intermediate zone, (*2*) fibers in the striatum, (*3*) anterior commissure, (*4*) thalamocortical axons, (*5*) fibers in the tectum, (*6*) medial lemniscus, (*7*) fasciculus retroflexus, (*8*) mammillothalamic tract, (*9*) corticospinal tract, (*10*) aberrant fibers surrounding the globus pallidus, and (*11*) aberrant fibers within the external capsule. Throughout this study, orange arrowheads indicate missing axons/tracts; white arrowheads (in contrast with white arrows) and red arrows (in contrast with green arrows) indicate fiber tracts with defects [misrouted or diminutive or, in rare cases, poorly fasciculated (arrow *6* in *E* vs. arrowhead *6* in *E*′)]. GP, globus pallidus. (Scale bars: *E*′, 1 mm; *G*′, 200 μm.) (*H*–*N*′) Thalamocortical axons labeled by AP staining of consecutive coronal sections from E18.5 *RORα-IRES-Cre*;*R26iAP*;$Fz3^{+/-}$ and *RORα-IRES-Cre*;*R26iAP*;$Fz3^{-/-}$ brains. In the $Fz3^{-/-}$ brain, most thalamocortical axons descend ventrally and then form a U-shaped axon tract to innervate the contralateral thalamus (*M*′ and *N*′) or project laterally to the cortical marginal zone (*J*′–*L*′). Complete brain sections in *M*–*N*′ show the U-shaped thalamocortical tracts in the $Fz3^{-/-}$ brain. (Scale bars, 1 mm.) (*O* and *P*) Planes of sections in *A*–*N*′. (*Q*) Schematics showing trajectories of thalamocortical axons in WT (*Left*) and $Fz3^{-/-}$ (*Right*) brains. In the $Fz3^{-/-}$ brain, thalamocortical axons from the left and right hemibrains are drawn in red and blue, respectively, for better illustration of the reciprocal innervation from the contralateral thalamus.

Fig. S1 *A′–E′*). In contrast, when *Fz3* was deleted exclusively in the dorsal thalamus (*RORα-IRES-Cre*;*Fz3*$^{CKO/-}$) or in the midbrain and hindbrain (*Dbx1-IRES-Cre*;*Fz3*$^{CKO/-}$), no defects in axon tracts were observed (Fig. 2 *E–F″*). We note that, in these and other experiments in which Cre-mediated deletion of the *Fz3*^{CKO} allele failed to produce a phenotype, any inferences regarding the dispensability of *Fz3* action in the region in question must be considered tentative because (*i*) the onset of *Cre* expression could be delayed relative to the time window of *Fz3* action or (*ii*) the level of *Cre* expression could be insufficient to eliminate *Fz3* from a large enough fraction of the relevant cells.

When *Fz3* was ablated in the neocortex (*Emx1-IRES-Cre*; *Fz3*$^{CKO/-}$), the posterior part of the anterior commissure was completely missing and axons with aberrant trajectories appeared in the external capsule (Fig. 2 *C–C″* and Fig. S1 *A″–E″*). As other CNS axon tracts appear to be unaffected in *Emx1-IRES-Cre*;*Fz3*$^{CKO/-}$ mice, it is likely that cortical axons that would normally have formed the posterior part of the anterior commissure constitute the aberrant axons in the external capsule. With the caveats noted earlier regarding the timing and efficiency of Cre-mediated recombination, these observations suggest that *Fz3* expression may not be required in all cortical and thalamic neurons for the development of the corticothalamic, corticospinal, and thalamocortical tracts.

The results described thus far are consistent with the possibility that corticothalamic, corticospinal, and thalamocortical axon pathfinding might require *Fz3* function in the structures through which these tracts pass. We tested this possibility by eliminating *Fz3* in the ventral telencephalon (*Dlx5/6-Cre*;*Fz3*$^{CKO/-}$) and observed that the corticothalamic, corticospinal, and thalamocortical tracts showed defects to various extents, with aberrant axon trajectories around the globus pallidus, disorganized axon bundles in the internal capsule, a subset of thalamocortical axons descending ventrally, and a diminished corticospinal tract (Fig. 2 *D–D″*). The most severely affected brains showed few or no axons linking the neocortex and the thalamus (Fig. 3 *A* and *B*). Many *Dlx5/6-Cre*;*Fz3*$^{CKO/-}$ mice survived to adulthood but were runted. In adult *Dlx5/6-Cre*;*Fz3*$^{CKO/-}$ brains, the lateral ventricles were markedly enlarged, and, in the striatum, presumptive corticothalamic and/or thalamocortical axons were bundled together and associated with activated astrocytes (Fig. 3 *C–D′*).

Taken together, these conditional ablation experiments showed that the most severe axon pathfinding phenotypes were produced when *Fz3* was deleted in all forebrain neurons (*Foxg1-Cre*) or only in ventral forebrain neurons (*Dlx5/6-Cre*), rather than in the cortical and thalamic neurons from which the axons originate. This pattern of phenotypes is strikingly similar to that obtained upon inactivation of a conditional allele of *Celsr3* with the same *Cre* drivers (18). This similarity argues for an intimate association between *Fz3* and *Celsr3* in forebrain axon pathfinding.

Corridor cells, a neuronal population derived from the lateral ganglionic eminence, form a permissive bridge for the growth of thalamocortical axons (19). The presence of corridor cells between the neocortex and the thalamus together with the essential role of *Fz3* in the ventral telencephalon raised the possibility that loss of *Fz3* might affect corridor cell development, migration, survival, or function. By immunostaining for Ebf1, a transcription factor expressed in corridor cells, we found that the distribution and abundance of corridor cells were very similar in E13.5 WT and *Fz3*$^{-/-}$ brains (Fig. 3 *E–F″*). The only apparent difference between genotypes was the presence of Ebf1^{+} cells at the medioventral face of the *Fz3*$^{-/-}$ globus pallidus, with the result that the *Fz3*$^{-/-}$ globus pallidus was completely encircled by corridor cells. Whether this difference in cellular distribution plays a causal role in, is a consequence of, or is unrelated to the misrouting thalamocortical axons in the *Fz3*$^{-/-}$ brain is unknown.

***Fz3* Is Required for the Normal Development of the Earliest Axon Tracts in the Mouse Brain.** In the vertebrate CNS, the first axon tracts develop in a stereotyped spatiotemporal pattern and serve as scaffolds for later growing axons (13). As a first step in determining whether *Fz3* plays a role in the development of the earliest CNS axon tracts, we examined their arrangement by NF immunostaining of whole-mount E12.5 heads (Fig. 4 *A* and *A′*). Although axon tracts in the brain were not as strongly labeled as were peripheral nerves, they could still be clearly identified. As seen in Fig. 4 *A* and *A′*, three major axon tracts (labeled I, II, and III) were arrested, greatly reduced in intensity, or absent in the *Fz3*$^{-/-}$ brain. In addition, the ventral branch of the trigeminal nerve (i.e., V3) was markedly thinned or completely missing in *Fz3*$^{-/-}$ embryos.

To more precisely identify the locations of the earliest axon tracts, serial sections of E11.5 and E12.5 heads were costained for NF and calbindin or calretinin, each of which labels distinctive populations of early born neurons that serve as useful landmarks (20). Calbindin^{+} neurons showed the same spatial

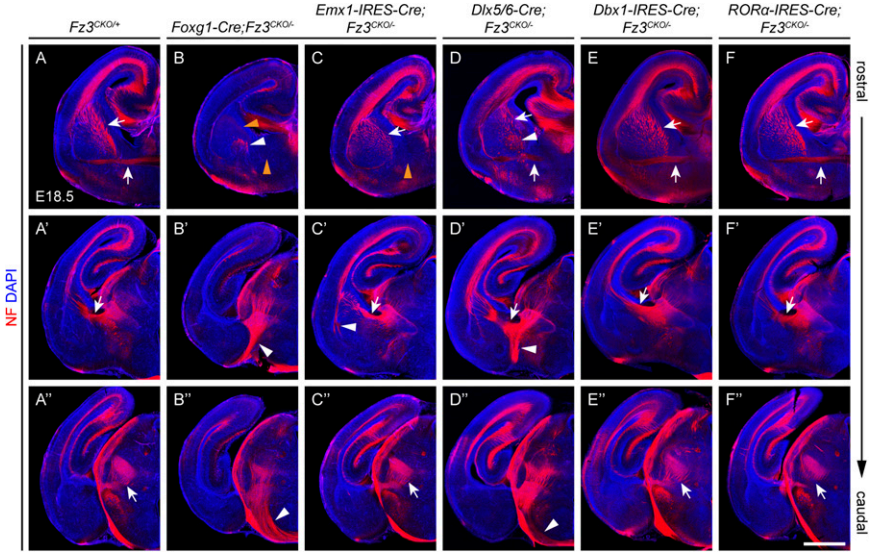

Fig. 2. The effect of region-specific inactivation of *Fz3* on the development of major axon tracts in prenatal mouse brains. (*A–F″*) NF immunostaining of coronal sections from E18.5 brains in which *Fz3* has been inactivated in the entire forebrain (*Foxg1-Cre*; *B–B″*), in the cerebral cortex (*Emx1-IRES-Cre*; *C–C″*), in the striatum (*Dlx5/6-Cre*; *D–D″*), in the midbrain and hindbrain (*Dbx1-IRES-Cre*; *E–E″*), and in the dorsal thalamus (*RORα-IRES-Cre*; *F–F″*). (*A–A″*) Phenotypically normal control sections. (*A–F*) Anterior commissure (lower arrows and arrowheads), axon tracts in the striatum (upper arrows and arrowhead), and aberrant axons surrounding the globus pallidus (middle white arrowheads in *B* and *D*). (*A′–F″*) More caudal images mainly show thalamocortical axons, except that the arrowhead in *C′* points to aberrant axon tracts within the external capsule. (Scale bar, 1 mm.)

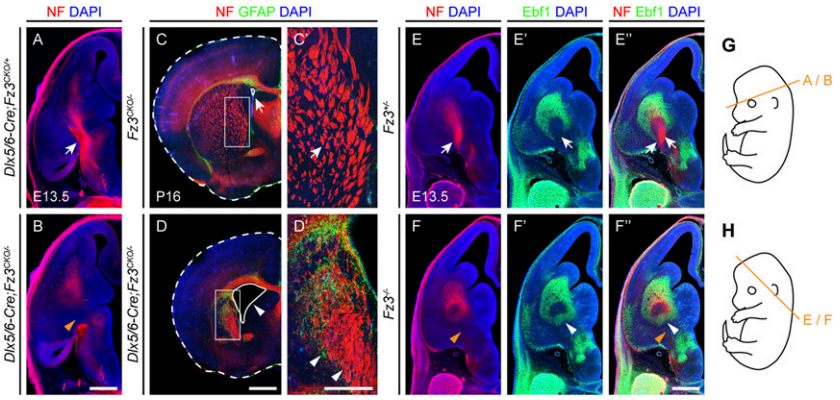

Fig. 3. Defects in embryonic and adult *Dlx5/6-Cre*; *Fz3*$^{CKO/-}$ brains and the effect of *Fz3* loss of function on corridor cells. (*A* and *B*) E13.5 *Dlx5/6-Cre*;*Fz3*$^{CKO/-}$ brain with no axonal connection between the thalamus and cerebral cortex (arrow in *A* vs. arrowhead in *B*), the most severe phenotype seen in *Dlx5/6-Cre*;*Fz3*$^{CKO/-}$ brains. (Scale bar, 500 μm.) (*C*–*D*′) Control vs. *Dlx5/6-Cre*; *Fz3*$^{CKO/-}$ brains at postnatal day (P) 16 showing NF and glial fibrillary acid protein immunostaining in coronal sections. The *Dlx5/6-Cre*;*Fz3*$^{CKO/-}$ brain shows an enlarged lateral ventricle (arrow in *C* vs. arrowhead in *D*), closely bundled axons (right arrowhead in *D*′), and activated (i.e., glial fibrillary acid protein-expressing) astrocytes (left arrowhead in *D*′) in the striatum. Dashed lines delineate the edge of the brain (*C* and *D*); the continuous white lines encircle the lateral ventricle (*C* and *D*). (*C*′ and *D*′) Magnified views of boxed regions in *C* and *D*, respectively. (Scale bars: *D*, 1 mm; *D*′, 500 μm.) (*E*–*F*″) NF and Ebf1 immunostaining of E13.5 brain sections showing in the *Fz3*$^{-/-}$ brain Ebf1^{+} corridor cells encircling the globus pallidus (arrows in *E*′ and *E*″ vs. arrowheads in *F*′ and *F*″) and thalamocortical axons missing from the internal capsule (arrow in *E* vs. arrowhead in *F*). (Scale bar, 500 μm.) (*G* and *H*) Planes of sections in *A*, *B*, *E*, and *F*.

distribution in *Fz3*$^{+/-}$ and *Fz3*$^{-/-}$ brains at E12.5 (Fig. 4 *J*–*R* vs. Fig. 4 *J*′–*R*′). In calbindin and NF double-stained sections, several axon tracts—along the lateral wall of the diencephalon (axon tract II; Fig. 4 *K*–*M*; upper arrows), connecting the diencephalon and the ventrolateral telencephalon (axon tract I; Fig. 4 *J*–*M*, lower arrows), and ascending from the brainstem to the midbrain (axon tract III; Fig. 4 *P*–*R*, arrows)—were missing or dramatically attenuated in the *Fz3*$^{-/-}$ brain.

In contrast to the unchanged distribution of calbindin^{+} neurons, the spatial distribution of calretinin^{+} immunoreactivity shows two clear differences between *Fz3*$^{+/-}$ and *Fz3*$^{-/-}$ brains at E11.5, both of which are associated with differences in axon trajectories. The first of these is shown in the center of Fig. 4 *E*–*H*′ and in Fig. S2 *E*–*L*′, in which two different planes of section through the same region of the *Fz3*$^{-/-}$ midbrain show a bundle of rostrally growing axons abutting a contiguous zone of calretinin^{+} cells (axon tract I, medial forebrain bundle). The corresponding region of the *Fz3*$^{+/-}$ midbrain shows the same axon bundle passing between two separated zones of calretinin^{+} neurons (Fig. 4*H*). The spatial relationship between axon bundles and calretinin^{+} neurons in the *Fz3*$^{+/-}$ brain suggests that the territories marked by calretinin^{+} neurons are nonpermissive for axon growth. In an extension of this hypothesis, the presence of the contiguous zone of calretinin^{+} neurons in the *Fz3*$^{-/-}$ midbrain may have blocked the growth of the axon bundle (Fig. 4*H*′). We note that the images are also consistent with a model in which the cessation of axon growth in the *Fz3*$^{-/-}$ midbrain occurred independently and permitted the separate territories of calretinin^{+} neurons to subsequently coalesce.

The second example of a difference in axon growth and calretinin^{+} immunoreactivity at E11.5 is seen at the top of Fig. 4 *E*–*G*′ and in Fig. S2 *A*–*D*′, where a cluster of calretinin^{+} neurons in the developing diencephalon is associated with a rostrally directed axon bundle in the *Fz3*$^{+/-}$ control brain (axon tract II, calretinin^{+} fiber tract in the thalamic eminence) that is absent in the *Fz3*$^{-/-}$ brain. The dependence of this axon bundle on *Fz3* was confirmed by selectively labeling it with AP in horizontal sections of E13.5 *Calb2-IRES-Cre*;*R26iAP*;*Fz3*$^{-/-}$ and *Calb2-IRES-Cre*; *R26iAP*;*Fz3*$^{+/-}$ brains (*Calb2* is the gene encoding calretinin; Fig. S3 *A*–*F*′). The failure of the diencephalic calretinin^{+} neurons to produce this axon bundle in the *Fz3*$^{-/-}$ brain at E11.5 implies an essential role for *Fz3* at the earliest stage in the development of diencephalic projections. At E13.5, calretinin^{+} neurons occupy the anterior thalamus (Fig. S3 *E*–*G*′). In the *Fz3*$^{+/-}$ brain these neurons are the source of calretinin^{+} thalamocortical axons (Fig. 4*I*). By contrast, no calretinin^{+} axons are observed in the internal capsule in the *Fz3*$^{-/-}$ brain (Fig. 4*I*′), consistent with the generalized defect in thalamocortical projections illustrated in Fig. 1.

To test whether deletion of *Fz3* selectively in calretinin^{+} neurons alters thalamocortical axon development, we generated *Calb2-IRES-Cre*;*Fz3*$^{CKO/-}$ and *Calb2-IRES-Cre*;*Fz3*$^{CKO/+}$ embryos. As seen in Fig. S3 *G*–*I*′, *K*, and *L*, embryos of both genotypes have calretinin^{+} and NF^{+} thalamocortical axons that are correctly positioned within the internal capsule at E13.5, and there was no difference between genotypes in the overall appearance of the thalamocortical projections at E15.5. With the caveats noted earlier regarding the timing and efficiency of Cre-mediated recombination, these observations suggest that *Fz3* expression may not be required in calretinin^{+} thalamic neurons for the development of the thalamocortical tract.

Autonomous and Nonautonomous Roles of *Fz3* in RGC Axon Guidance. *Fz3* is expressed in the developing mouse retina (6), but it is not known whether *Fz3* plays a role in retinal development or RGC axon growth and guidance. To assess the trajectories of RGC axons, we combined a retina-specific *Pax6α-Cre* transgene, which efficiently recombines target loci beginning at E9.5 (21), with a *Brn3b*^{CKOAP} allele in which an AP reporter inserted 3′ of the *Brn3b* transcription termination site is expressed following Cre-mediated deletion of both *Brn3b* exons (22). *Brn3b* is expressed by the majority of RGCs, and therefore the majority of RGC axons can be visualized by AP histochemistry in *Pax6α-Cre*; *Brn3b*$^{CKOAP/+}$ brains.

As seen in *Pax6α-Cre*;*Brn3b*$^{CKOAP/+}$ (i.e., WT) brains, central targets of RGC axons include the lateral geniculate nucleus and the medial terminal nucleus (MTN; Fig. 5 *A*–*E*). In *Pax6α-Cre*; *Brn3b*$^{CKOAP/+}$;*Fz3*$^{-/-}$ brains, the optic nerves and optic chiasm were unaffected, but two defects were observed: (*i*) caudal to the optic chiasm, a subset of optic tract axons diverged from their normal trajectories and entered the medial thalamus and (*ii*) projections to the MTN were missing (Fig. 5 *A*′–*E*′). As shown in Fig. 1*D*′, in the *Fz3*$^{-/-}$ thalamus, misrouted thalamocortical axons form a massive U-shaped bundle that courses adjacent to the optic tract along the ventral and lateral boundaries of the thalamus. To determine whether some of the divergent optic tract axons were cofasciculating with these misrouted intrathalamic axons, we visualized RGC axons by immunostaining for AP and all axons by immunostaining for NF in coronal sections from *Pax6α-Cre*;*Brn3b*$^{CKOAP/+}$;*Fz3*$^{+/-}$ and *Pax6α-Cre*; *Brn3b*$^{CKOAP/+}$;*Fz3*$^{-/-}$ brains. This analysis shows some RGC axons in the *Pax6α-Cre*;*Brn3b*$^{CKOAP/+}$;*Fz3*$^{-/-}$ brain in close contact with misrouted thalamocortical axons (Fig. 5 *L*–*N*).

To address the question of whether the aberrant trajectories of *Fz3*$^{-/-}$ RGC axons reflect (*i*) an autonomous requirement for

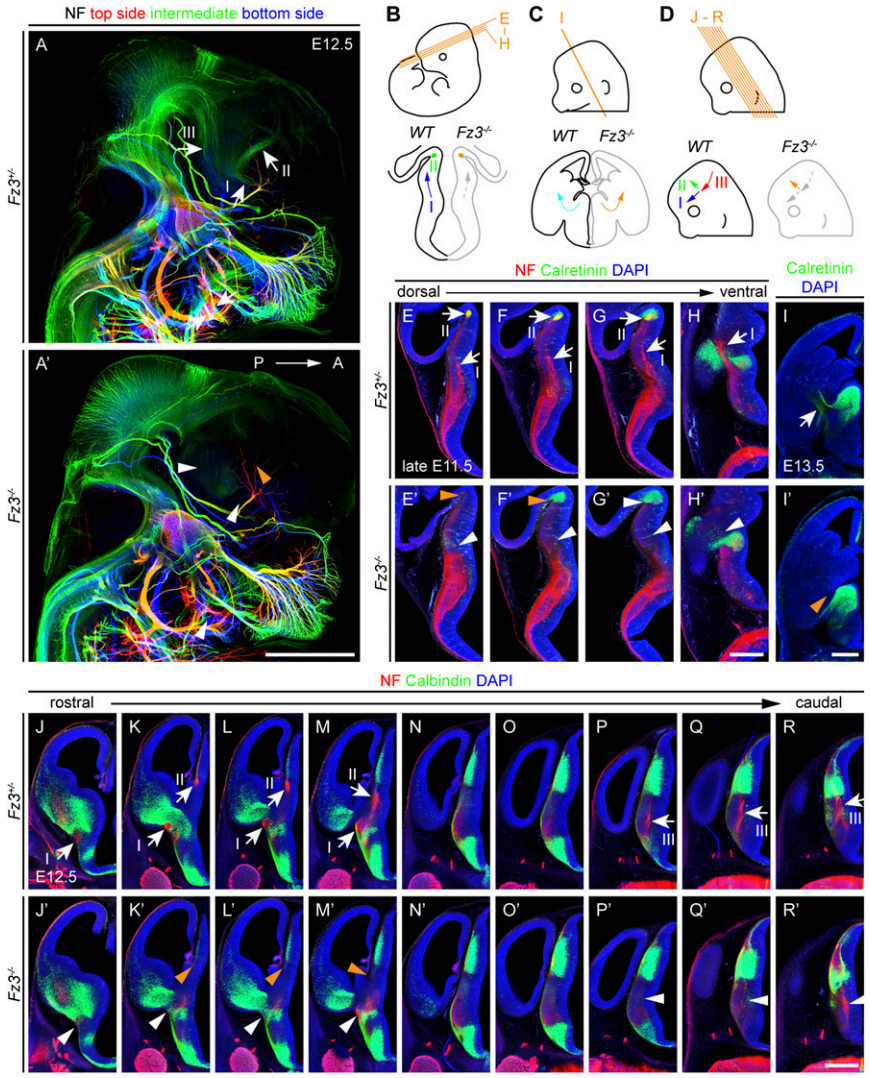

Fig. 4. Several early developing axon tracts are disrupted in the *Fz3*$^{-/-}$ brain. (*A* and *A′*) NF immunostaining of E12.5 whole-mount heads in lateral view showing a complete or nearly complete absence of the three most prominent axon tracts in the brain (numbered I, II, and III; upper three arrows in *A* vs. arrowheads in *A′*) and the ventral branch of the trigeminal nerve (V3) in *Fz3*$^{-/-}$ embryos (lower pair of arrows in *A* vs. arrowhead in *A′*). Axon tract I is the medial forebrain bundle originating from the midbrain and ascending to the basal forebrain; axon tract II is the calretinin^{+} fiber tract in the thalamic eminence; and axon tract III originates from the brainstem and projects rostrally. The axons are color coded to represent depth within the *Z*-stack, with red representing superficial axons on the near side, green representing axons in the center, and blue representing superficial axons on the far side. A, anterior; P, posterior. (Scale bar: 500 μm.) (*B–D*) Planes of sections in *E–H′* (*B*), *I* and *I′* (*C*), and *J–R′* (*D*), and summary comparisons of axon tracts (*Lower*): axon tracts in WT (colored arrows and dot, left side of drawings) vs. defective counterparts in *Fz3*$^{-/-}$ brains (gray dashed or orange arrows and orange dot, right side of drawings). The green dot in *B* and green arrow in *D* represent tract II; the lower blue arrows in *B* and *D* represent tract I; the red arrow in *D* represents tract III; and the cyan arrow in *C* represents calretinin^{+} thalamocortical axons. In all schematic drawings, gray dashed arrows represent diminutive axon tracts, and orange arrows and dots represent completely missing axon tracts. (*E–H′*) NF and calretinin immunostaining of consecutive E11.5 brain sections showing the diminutive medial forebrain bundle (axon tract I, lower arrows vs. arrowheads in *E–H′*) and the absence of the calretinin^{+} axon tract in the thalamic eminence (axon tract II, top arrows vs. arrowheads in *E–G′*) in the *Fz3*$^{-/-}$ brain. (Scale bar, 500 μm.) (*I* and *I′*) Calretinin^{+} thalamocortical axons fail to enter the internal capsule in the E13.5 *Fz3*$^{-/-}$ brain (arrow vs. arrowhead), as seen in coronal sections. (Scale bar, 500 μm.) (*J–R′*) NF and calbindin immunostaining of consecutive E12.5 brain sections shows an unaltered distribution of calbindin^{+} neurons in the *Fz3*$^{-/-}$ brain, the diminutive medial forebrain bundle (axon tract I, lower arrows in *J–M* vs. lower arrowheads in *J′–M′*), the absence of the axon tract in the thalamic eminence (axon tract II, top arrows in *K–M* vs. top arrowheads in *K′–M′*), and the diminutive ascending fiber tract from the brainstem to the midbrain (axon tract III, arrows in *P–R* vs. arrowheads in *P′–R′*). (Scale bar, 500 μm.)

Fz3 function in RGCs, (*ii*) an interaction between RGC axons and misrouted thalamic axons, or (*iii*) a combination of the two, we generated *Pax6α-Cre*;*Brn3b*$^{CKOAP/+}$;*Fz3*$^{CKO/-}$ embryos in which *Fz3* was deleted in *hPLAP*-expressing RGCs but the rest of the CNS remained WT (Fig. 5 *F–K′*). In these mice, AP^{+} projections to the lateral geniculate nucleus and superior colliculus showed no pathfinding defects, implying that the misrouting of optic tract axons within the *Fz3*$^{-/-}$ thalamus is not a cell-autonomous process, but most likely arises from inappropriate fasciculation with misrouted intrathalamic axons. In contrast, AP^{+} projections to the MTN were greatly attenuated in *Pax6α-Cre*;*Brn3b*$^{CKOAP/+}$;*Fz3*$^{CKO/-}$ brains, implying that MTN targeting requires *Fz3* function within RGC axons or growth cones. The small number of RGC axons in *Pax6α-Cre*;*Brn3b*$^{CKOAP/+}$;*Fz3*$^{CKO/-}$ brains that project to the MTN could derive from RGCs that have recombined the *Brn3b*^{CKOAP} allele but not the *Fz3*^{CKO} allele, a plausible scenario given that *Pax6α-Cre* expression progressively declines within the lateral and nasal retina (21).

We next asked whether *Fz3* is involved in retinal lamination, a major organizing feature for retinal circuitry. To address this question, we analyzed retinas from adult *Six3-Cre*;*Fz3*$^{CKO/-}$ mice. The *Six3-Cre* transgene is expressed throughout the retina starting at approximately E11 (23), but its expression in the brain is sufficiently limited that *Six3-Cre*;*Fz3*$^{CKO/-}$ mice survive to adulthood. In cross-sections of *Six3-Cre*;*Fz3*$^{CKO/-}$ retinas, the overall organization of the retina appeared unaltered, and, as shown in Fig. S4, GABAergic, dopaminergic, cholinergic, calbindin^{+}, and calretinin^{+} amacrine cells were present in their correct abundances and locations and exhibited normal patterns of dendritic stratification within the inner plexiform layer. These observations rule out a major role for *Fz3* in retinal development.

Effects of *Fz3* KO on the Growth and Guidance of Catecholaminergic and Serotonergic Axons. In the mammalian brain, neuromodulatory systems that use low molecular weight neurotransmitters—acetylcholine, dopamine, epinephrine, norepinephrine, histamine, and serotonin—are characterized by diffuse projections from the ventral forebrain and/or brainstem to multiple target areas. The initial description of the *Fz3*$^{-/-}$ axon guidance phenotype noted the failure of midbrain dopaminergic axons to arrive at the striatum, and subsequent experiments have demonstrated defects in cell body orientation and axon trajectories among dopaminergic and serotonergic neurons (6, 24). To assess these defects in more detail, we have characterized dopaminergic

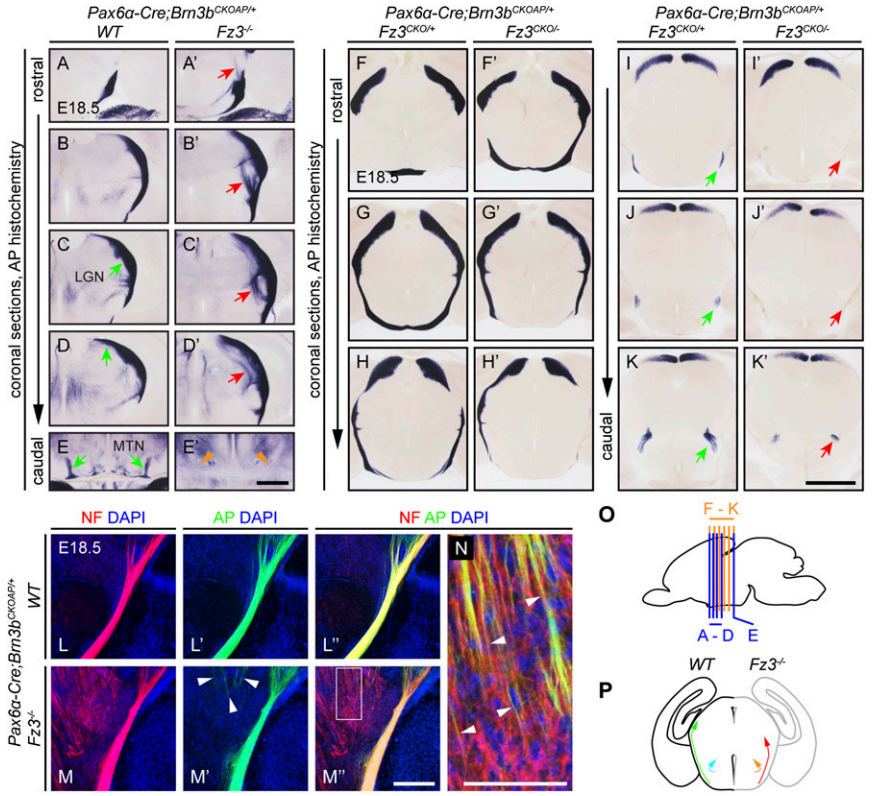

Fig. 5. Defects in the central projections of *Fz3*$^{-/-}$ RGC axons. (*A–E′*) AP^{+} RGC axons from *Pax6α-Cre*; *Brn3b*$^{CKOAP/+}$ mice at E18.5. In the *Fz3*$^{-/-}$ brain, some RGC axons in the thalamus diverge from the optic tract (red arrows in *A′–D′*), and the MTN is not innervated (green arrows in *E* vs. orange arrowheads in *E′*). LGN, lateral geniculate nucleus. (Scale bar, 500 μm.) (*F–K′*) AP^{+} RGC axons in *Pax6α-Cre;Brn3b*$^{CKOAP/+}$; *Fz3*$^{CKO/-}$ mice at E18.5 exhibit normal trajectories except for a reduced projection to the inferior fasciculus and MTN (green vs. red arrows in *I–K′*). (Scale bar, 1 mm.) (*L–N*) NF and AP immunostaining of coronal sections of an E18.5 *Pax6α-Cre;Brn3b*$^{CKOAP/+}$; *Fz3*$^{-/-}$ thalamus showing misrouted AP^{+}/NF^{+} RGC axons cofasciculating with aberrant and ventrally directed NF^{+}/AP^{-} thalamic axons (arrowheads in *M′* and *N*). (*N*) Enlarged view of the boxed region in *M″*. (Scale bars: *M″*, 200 μm; *N*, 100 μm.) (*O*) Planes of sections in *A–K′*. (*P*) The green arrow (*Left*) shows the trajectory of the optic tract in the WT brain, and the red arrow (*Right*) shows the medial misrouting of some optic tract axons in the *Fz3*$^{-/-}$ brain; the cyan arrow at left shows the innervation of the MTN by optic tract axons in the WT brain, and the orange arrow at right shows the absence of MTN innervation by optic tract axons in the *Fz3*$^{-/-}$ brain.

and serotonergic projections at E13.5 and E16.5 or E18.5 by using anti-TH (adrenergic, noradrenergic, and dopaminergic) and anti–5-HT (serotonergic) immunolabeling.

In WT brains, TH^{+} axons extend ∼2 mm anteriorly from their origin in the midbrain at E13.5 (Fig. 6 *A–J*), and are present at high density in the striatum at E18.5 (Fig. 6 *L* and *M*). In contrast, in *Fz3*$^{-/-}$ brains, TH^{+} axons extend only ∼0.5 mm anteriorly at E13.5 (Fig. 6 *A′–J′*) and are present at low density in the striatum at E18.5 (Fig. 6 *L′* and *M′*). In WT and *Fz3*$^{-/-}$ embryos, numerous anteriorly directed TH^{+} axons are seen at E18.5 in the midbrain and diencephalon (Fig. 6 *N* and *N′*), with many axons appearing less well organized along the rostrocaudal axis in the *Fz3*$^{-/-}$ brain (Fig. 6*N′*, red arrows). Strikingly, in *Fz3*$^{-/-}$ brains, there is a large and aberrant TH^{+} axon tract coursing caudally from the midbrain along the ventral surface of the medulla (Fig. 6 *O* and *O′*). These observations were confirmed with the use of a more specific genetic marking system based on *Cre* expression from the Dopamine transporter-1 (*Dat1*) locus (25). As *Dat1* is expressed exclusively in dopaminergic neurons, analyses based on *Dat1-Cre* are not confounded by signals from adrenergic and noradrenergic axons. Fig. 6 *P–Q′* and Fig. S5 show the full trajectories of dopaminergic axons in *Dat1-Cre;R26iAP;Fz3*$^{+/-}$ (WT) and *Dat1-Cre;R26iAP;Fz3*$^{-/-}$ brains at E18.5. These data demonstrate that, in the *Fz3*$^{-/-}$ brain, few if any midbrain dopaminergic axons reach the striatum and numerous dopaminergic axons project to the spinal cord.

Anti–5-HT immunostaining of E13.5 WT and *Fz3*$^{-/-}$ embryos showed that serotonergic axons in the *Fz3*$^{-/-}$ brainstem fail to project rostrally beyond the midbrain (Fig. 7 *A–J′*). A sagittal view of the entire brain at E16.5 shows normal 5-HT^{+} axons in the tegmentum (Fig. 7 *L* and *L′*, arrows), but a complete absence of 5-HT^{+} axons in the cerebral cortex and striatum (Fig. 7 *M–N′*) and an aberrant 5-HT^{+} axon tract coursing caudally along the ventral medulla (Fig. 7 *O* and *O′*), a pattern that closely resembles the defects described above for dopaminergic axons in the *Fz3*$^{-/-}$ brain. These data confirm and extend the earlier work of Wang et al. (6) and Fenstermaker et al. (24), and show that loss of *Fz3* leads to a severe defect in the asymmetric rostrocaudal orientation of dopaminergic and serotonergic axons.

Absence of the Spinothalamic Tract in *Fz3*$^{-/-}$ Mice: Functional Consequences. Loss of *Fz3* leads to impaired rostral turning by growth cones of spinal cord commissural sensory axons at midgestation (8). To define the neuroanatomic consequences of this guidance defect later in gestation, we visualized ascending axons in WT and *Fz3*$^{-/-}$ brains by combining the *R26iAP* reporter and a *Caudal-1* (*Cdx1*)-*Cre* transgene, which recombines target alleles in all tissues caudal to the upper thorax before midgestation (9, 26). As seen in Fig. 8 *A–M*, there is a large reduction in ascending axons in the brainstem and a complete absence of ascending axons in the midbrain and thalamus in *Fz3*$^{-/-}$ brains.

In previous work, we used *Cdx1-Cre* to eliminate *Fz3* in all cells in the trunk and limbs and found that, except for a curled tail and an odd gait—the result of a failure of motor axons to innervate the anterior compartment musculature of the lower hindlimb—adult *Cdx1-Cre;Fz3*$^{CKO/-}$ mice appear completely healthy (9). However, the absence of ascending spinal cord axons—and, in particular, the absence of the spinothalamic tract—in the *Fz3*$^{-/-}$ CNS suggested the interesting possibility that, despite their grossly normal appearance, *Cdx1-Cre;Fz3*$^{CKO/-}$ mice might lack the ability to transmit sensory information from the trunk and limbs to the brain.

Before embarking on a test of somatosensation in *Cdx1-Cre*; *Fz3*$^{CKO/-}$ mice, we first asked whether loss of *Fz3* affects the structure of peripheral sensory nerves. To selectively visualize sensory axons, we studied WT and *Fz3*$^{-/-}$ mice carrying an AP reporter knocked into the *Brn3a* gene, which is expressed in all or nearly all neurons in dorsal root ganglia and cranial sensory ganglia (22, 27). AP staining of horizontal sections from E15.5 *Brn3a*$^{AP/+}$;*Fz3*$^{+/-}$ and *Brn3a*$^{AP/+}$;*Fz3*$^{-/-}$ embryos showed no abnormalities in sensory nerve development or

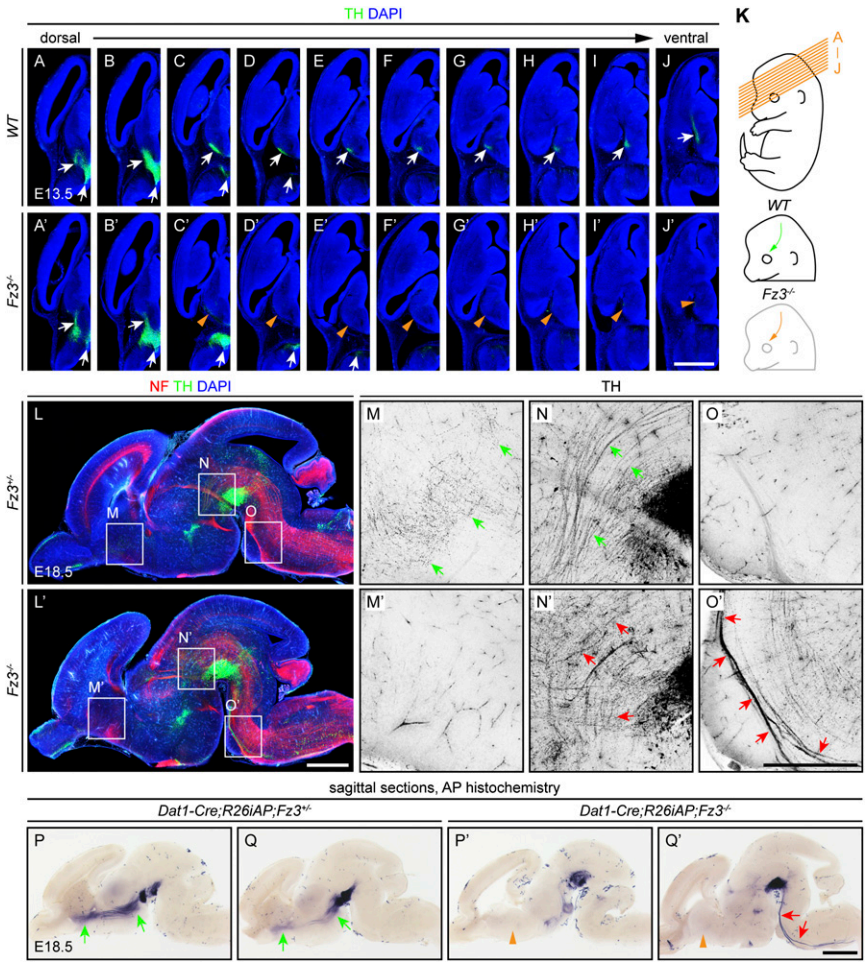

Fig. 6. Defects in the orientation and growth of midbrain dopaminergic axons in $Fz3^{-/-}$ embryos. (*A–J′*) In consecutive sections of WT and $Fz3^{-/-}$ brains at E13.5, midbrain TH^+ neurons are present (lower arrows in *A–D* and *A′–E′*), but, in the $Fz3^{-/-}$ brain, TH^+ axons do not project to the basal forebrain (top white arrows in *C–J* vs. orange arrowheads in *C′–J′*). (Scale bar: 1 mm.) (*K*) Planes of sections for *A–J′* (*Top*), trajectories of TH^+ axons in the E13.5 WT brain (green arrow; *Middle*), and missing axons in the E13.5 $Fz3^{-/-}$ brain (orange arrow; *Bottom*). (*L–O′*) NF and TH immunostaining of E18.5 sagittal brain sections showing that, in the $Fz3^{-/-}$ brain, the striatum is devoid of TH^+ axons (*M* vs. *M′*), some TH^+ axons project rostrally from the substantia nigra (*N* vs. *N′*), and other TH^+ axons descend to the spinal cord (*O* vs. *O′*). (*M–O′*) Enlarged views of boxed regions in *L* and *L′* showing only the anti-TH signal with intensity inverted. Background immunostaining is present in the vasculature. (Scale bars: *L′*, 1 mm; *O′*, 500 μm.) (*P–Q′*) In the *Dat1-Cre;R26iAP;*$Fz3^{-/-}$ brain, AP^+ dopaminergic axons do not innervate the striatum (green arrows in *P* and *Q* vs. orange arrowheads in *P′* and *Q′*) and form an aberrant tract that descends to the spinal cord (red arrows in *Q′*). (Scale bar, 1 mm.)

target innervation (Fig. S6). We also tested ambulation by using a rotarod. Although *Cdx1-Cre*;$Fz3^{CKO/-}$ mice walk awkwardly compared with WT controls, they are able to maintain their balance on a 6-cm-diameter rod rotating at 8 rpm (Movies S1 and S2).

On the assumption that primary somatosensation at the level of dorsal root ganglia neurons was largely or completely intact in *Cdx1-Cre*;$Fz3^{CKO/-}$ mice, we then asked whether somatosensory information from the spinal cord could be communicated to the brain by testing 1–3-mo-old *Cdx1-Cre*;$Fz3^{CKO/-}$ mice and their WT littermates in a pair of thermal and texture preference tasks. When WT mice are presented with a choice between surfaces held at 32 °C and 38 °C, they show a marked preference for the 32 °C surface. Similarly, when WT mice are presented with a choice between rough and smooth surfaces (60-grain and 400-grain sandpaper, respectively), they show a marked preference for the smooth surface. (Before performing the texture preference task, the mice had their whiskers trimmed; under these conditions, we presume that texture is sensed through their feet.) Independent experiments, performed in the dark with WT mice, demonstrated that texture preference does not depend on visual cues. These preferences are presumed to involve integration of sensory inputs at the level of the thalamus and higher cognitive centers. Strikingly, in these behavioral tests, *Cdx1-Cre*;$Fz3^{CKO/-}$ mice appeared to be largely or completely oblivious to differences in temperature and texture, whereas control littermates showed the expected preference for lower temperature and smoother texture (Fig. 8 *N* and *O* and Fig. S7). In comparing 10 trials with WT controls (two trials per mouse × five mice) and 15 trials with *Cdx1-Cre*;$Fz3^{CKO/-}$ mice (three trials per mouse × five mice), the *P* values for the preference differences between genotypes during each 30-min half of the 60-min trial were $P < 0.01$ and $P < 0.02$ for the texture and temperature tasks, respectively. Although we cannot rule out the possibility that the indifference shown by *Cdx1-Cre*;$Fz3^{CKO/-}$ mice to the different stimuli reflects an information-processing defect within the spinal cord, the most straightforward explanation for the anatomic and behavioral data is that temperature and texture preferences require supraspinal information processing. If correct, this explanation would imply that *Cdx1-Cre*;$Fz3^{CKO/-}$ mice inhabit a mental world without brain representations of somatosensory information from the trunk and limbs.

Discussion

The experiments reported here substantially extend earlier studies of *Fz3* action in the CNS. In particular, they show that ubiquitous loss of *Fz3* disrupts the growth and correct orientation of several axon tracts in the developing brain from the earliest times in their development (E11.5), produces large-scale anterior/posterior misrouting of midbrain dopaminergic and brainstem serotonergic axons, and leads to aberrant cofasciculation of optic and intrathalamic axon tracts. These experiments also show that loss of *Fz3* in cell populations along the route taken by thalamocortical axons perturbs the trajectories of these axons in a manner that is identical or nearly identical to the perturbations induced by loss of *Celsr3* in the same cell populations. Finally, these experiments show that selective deletion of *Fz3* in the trunk and limbs results in an adult nervous system in which most,

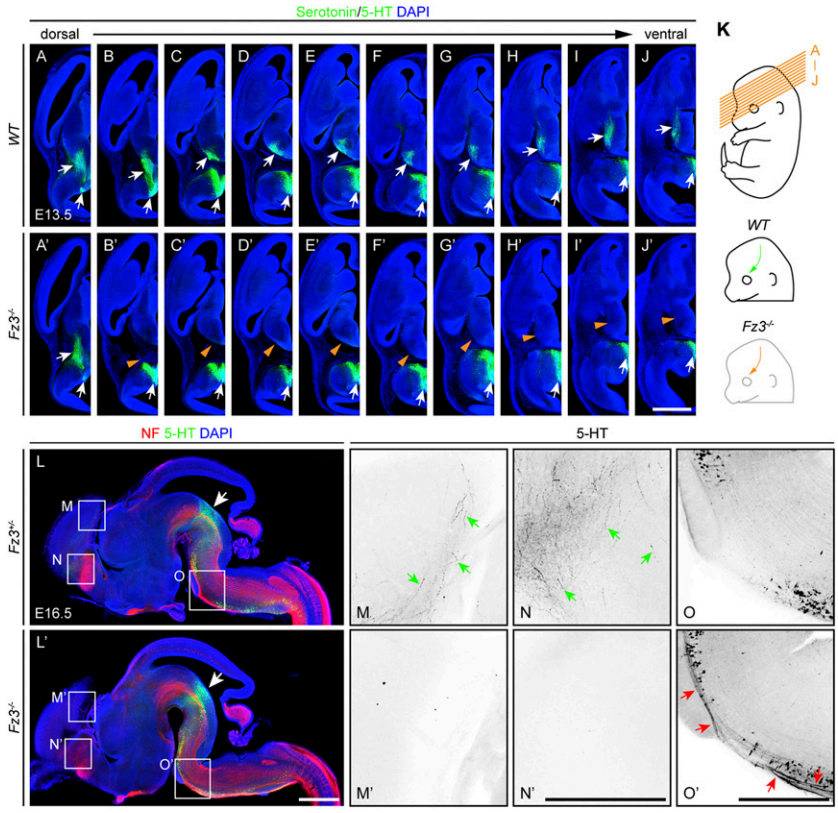

Fig. 7. Defects in the orientation and growth of serotonergic axons in *Fz3*$^{-/-}$ embryos. (*A–J′*) In WT and *Fz3*$^{-/-}$ brains, brainstem serotonergic neurons are present (lower arrows in *A–J* and *A′–J′*), but, in the *Fz3*$^{-/-}$ brain, serotonergic axons do not project rostrally (upper white arrows in *B–J* vs. orange arrowheads in *B′–J′*), shown by immunostaining for 5-HT on consecutive E13.5 brain sections. (Scale bar, 1 mm.) (*K*) Planes of sections for *A–J′* (*Top*), trajectories of serotonergic axons in the E13.5 WT brain (green arrow; *Middle*), and missing axons in the E13.5 *Fz3*$^{-/-}$ brain (orange arrow; *Bottom*). (*L–O′*) NF and 5-HT immunostaining of E16.5 sagittal brain sections showing that in the *Fz3*$^{-/-}$ brain the cortex and striatum are devoid of serotonergic axons (arrows in *M* and *N* vs. *M′* and *N′*), and numerous serotonergic axons descend along the ventral medulla (arrows in *O′*). (*M–O′*) Enlarged views of boxed regions in *L* and *L′* showing only the anti-5-HT signal with intensity inverted. Arrows in *L* and *L′* point to the tegmentum. (Scale bars: *L′*, 1 mm; *N′* and *O′*, 500 μm.)

if not all, ascending spinal sensory axons are missing, permitting an analysis of brain structure and function in the absence of sensory input from the lower body.

PCP Genes and the Control of Axon Growth and Guidance. As noted earlier, the identity or near-identity of phenotypes in comparisons of constitutive *Fz3* and *Celsr3* mutations and of conditional *Fz3* and *Celsr3* mutations in the cortex (*Emx1-Cre*) or ventral telencephalon (*Dlx5/6-Cre*) argues that these two integral membrane PCP proteins are likely to be involved in the same axon signaling mechanism(s) (5, 6, 18, 28). In epithelia, Frizzled and Celsr/Fmi/Stan proteins are partially colocalized, with Frizzled localized to one face of each epithelial cell and Celsr/Fmi/Stan localized to that face and to the opposite face of the cell (29). A critical and still open question is whether axon guidance involves homophilic Celsr/Fmi/Stan complexes between neighboring cells, as appears to be the case for the transfer of epithelial polarity information.

In several regions in the CNS, axons that are dependent on Fz3 exhibit alternate trajectories when Fz3 is missing. Thus, thalamic axons are rerouted to the contralateral thalamus and the ventral telencephalon, and many midbrain dopaminergic and brainstem serotonergic axons are rerouted caudally to the medulla and spinal cord. These observations suggest that there is a hierarchy of default trajectories, and they also emphasize the point that loss of *Fz3* does not affect axon growth per se. A different axon phenotype was recently described in the *Fz3*$^{-/-}$ dorsal limb in which motor axons stall at a discrete location within the nerve plexus at the base of the limb (9). Motor axon growth proximal to the stalling point was essentially normal, so this phenotype also is unlikely to represent a defect in axon growth. These distinct patterns of defective axon growth and guidance indicate that different axons respond differently to defects in Fz3 signaling, perhaps because interactions with other guidance cues modify the response to Fz3 signals.

The defect in thalamocortical axon guidance in *Dlx5/6-Cre*; *Fz3*$^{CKO/-}$ mice implies that Fz3/Celsr3 signaling plays an essential role in cell populations, such as corridor cells, that line the route through which these axons pass. Although more refined *Cre* drivers will be required to precisely define the relevant cell population in which Fz3 and Celsr3 act in the ventral telencephalon, these data already reveal an added layer of complexity, as earlier work using CNS-specific deletion of *Fz3* in the spinal cord indicated that motor axon growth in the dorsal limb does not require *Fz3* expression in peripheral tissues along the route through which motor axons pass in WT limbs and within which they stall in the *Fz3*$^{-/-}$ limb (9).

Brain Function Without Ascending Sensory Information. Somatosensory information from the limbs and trunk is conveyed to the brain via anatomically distinct spinal pathways (30). Pain, temperature, and crude touch are conveyed by the anterolateral pathway, which projects to the brainstem reticular formation, midbrain tectal nuclei, and thalamus. Tactile and proprioceptive information is conveyed by the dorsal column-medial lemniscal system, which projects to the thalamus. Additional pathways, such as the spinocerebellar pathway, convey information to subcortical structures to regulate reflex responses and fine tune voluntary movements. The temperature and texture preferences displayed by WT mice (Fig. 8 *N* and *O*) require (*i*) a differentiation of two innocuous stimuli based on afferent information from the soles of the feet, (*ii*) a decision to seek out one of the stimuli and/or avoid the other, and (*iii*) a set of motor commands to execute the decision. It is very likely that successful completion of this task requires information processing by the somatosensory and frontal regions of cortex, and therefore a relay of sensory information from spinal cord to thalamus to cortex. Based on the behavioral and anatomic data, it seems unlikely that any somatosensory

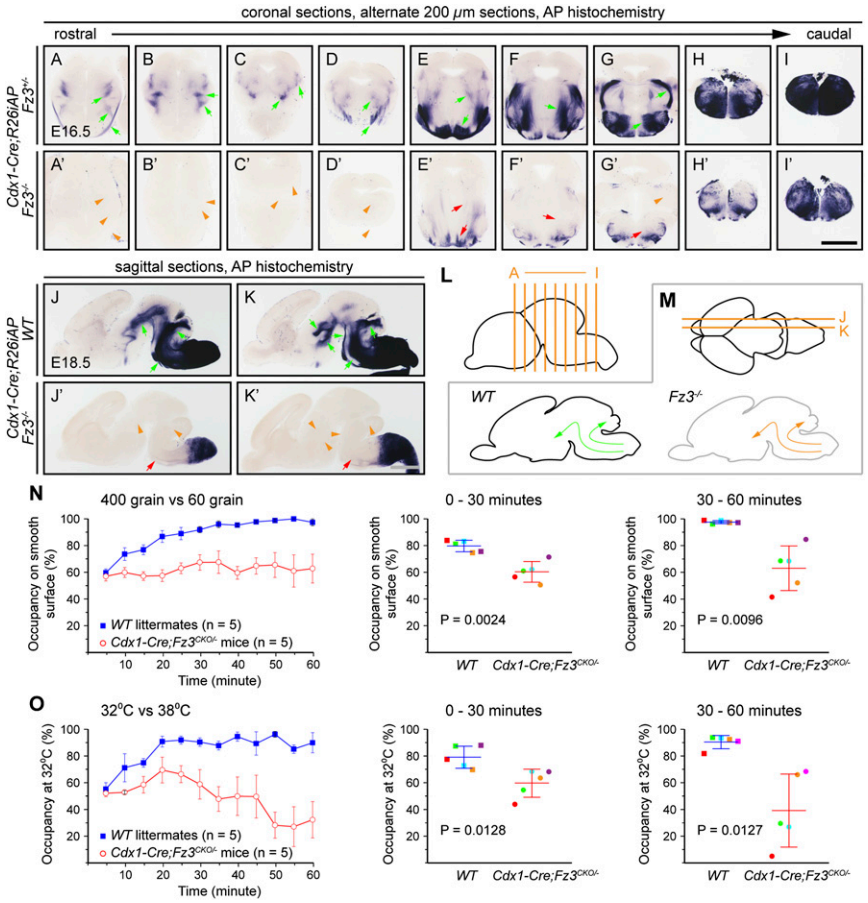

Fig. 8. Ascending axon tracts from the spinal cord are missing in the *Fz3*$^{-/-}$ brain, and *Cdx1-Cre;Fz3*$^{CKO/-}$ mice show no texture or temperature preferences when stimuli are delivered to their feet. (*A–K′*) AP^{+} ascending axon tracts from the spinal cord to the brain in E16.5 coronal (*A–I′*) and E18.5 sagittal (*J–K′*) brain sections from embryos carrying the *R26iAP* reporter recombined by the *Cdx1-Cre* transgene (green arrows in *A–G*, *J*, and *K*). These axons are largely missing in *Fz3*$^{-/-}$ brains (orange arrowheads in *A–D′*, *G′*, *J′*, and *K′* show missing axon tracts, and red arrows show diminutive tracts). (Scale bars: 1 mm.) (*L*) Planes of sections in *A–I′*. (*M*) Planes of sections in *J–K′* (*Upper*), and ascending spinal cord axon tracts in the WT brain (green arrows; *Left*) are missing in the *Fz3*$^{-/-}$ brain (orange arrows; *Right*). (*N*) Texture preference test results for WT (blue) and *Cdx1-Cre;Fz3*$^{CKO/-}$ mice (red) for smooth (400-grain sandpaper) vs. rough (60-grain sandpaper) surfaces over 60 min. For each genotype, five age-matched mice consisting of three males and two females were tested. Each WT mouse was tested twice, and each *Cdx1-Cre;Fz3*$^{CKO/-}$ mouse was tested three times. (*Left*) The percent of the time spent on the smooth surface is shown as the mean ± SEM for each 5-min interval. (*Right*) The percent of the time spent on the smooth surface is shown for the first and second 30-min intervals as the mean ± SD; each of the five colored dots represents a different mouse. For statistical analyses, the test results for each mouse were first averaged. WT mice show a strong preference for the smooth surface. *Cdx1-Cre;Fz3*$^{CKO/-}$ mice show no preference. (*O*) Thermal preference test results for WT (blue) and *Cdx1-Cre;Fz3*$^{CKO/-}$ mice (red) for 32 °C vs. 38 °C surfaces over 60 min (mean ± SEM). Data are displayed as described for the texture preference data in *N*. Each WT mouse was tested twice, and each *Cdx1-Cre;Fz3*$^{CKO/-}$ mouse was tested three times. WT mice show a strong preference for the 32 °C surface. *Cdx1-Cre;Fz3*$^{CKO/-}$ mice show no preference.

information from the trunk and limbs is being transmitted to the *Cdx1-Cre;Fz3*$^{CKO/-}$ thalamus and cortex. However, we cannot rule out the possibility that a small minority of ascending sensory axons in the *Cdx1-Cre;Fz3*$^{CKO/-}$ spinal cord are impervious to the effects of *Fz3* inactivation or that some neurons that relay ascending information escape Cre-mediated recombination. Because the medulla straddles the boundary of Cre^{+} and Cre^{-} territories (Fig. 8 *A–K′*), the first consideration is most relevant for axons that project to the medulla and the second consideration is most relevant for neurons that reside in the medulla.

Despite their somatosensory deficiencies, the ambulatory ability of *Cdx1-Cre;Fz3*$^{CKO/-}$ mice—although partially compromised by a lower hindlimb motor innervation defect—appears to be substantially intact. This might seem surprising, as the defect in ascending spinal projections likely blocks the transmission of proprioceptive information to the brain. However, a large body of work on intrinsic spinal cord locomotor circuits demonstrates that for many reflex responses somatosensory information is integrated into locomotor programs at the level of spinal circuits with little or no involvement of supraspinal mechanisms (31, 32). Moreover, the sparing of sensory axons in the head in *Cdx1-Cre;Fz3*$^{CKO/-}$ mice implies that vestibular, whisker, and visual inputs should be integrated normally to modulate descending motor commands to the spinal cord.

It would be interesting to test *Cdx1-Cre;Fz3*$^{CKO/-}$ mice for their responses to other somatosensory stimuli, such as itch and surface-borne vibration. It would also be interesting to examine the anatomy and physiology of neurons in the thalamus and somatosensory cortex in *Cdx1-Cre;Fz3*$^{CKO/-}$ mice to explore the fate of territories that normally process somatosensory information from the trunk and limbs. One might anticipate that there would be a large scale remapping of these territories analogous to the remapping of visual cortex in humans or animals that are congenitally blind (33–35).

Materials and Methods

The following mouse lines were used: *Brn3a*^{CKOAP} (22), *Brn3b*^{CKOAP} (22), *Cdx1-Cre* (26), *Fz3*$^{-/-}$ (6), *Fz3*$^{CKO/CKO}$ (9), *Calb2-IRES-Cre* (010774; Jackson Laboratory) (36), *Dat1-Cre* (25), *Dbx1-IRES-Cre* (031751-MU; Mutant Mouse Regional Resource Centers), *Dlx5/6-Cre* (16), *Emx1-IRES-Cre* (15), *Foxg1-Cre* (17), *Pax6α-Cre* (21), *RORα-IRES-Cre* (10), *R26iAP* (11), and *Sox2-Cre* (37). Mice were handled and housed in accordance with institutional animal care and use committee guidelines of the Johns Hopkins Medical Institutions.

Alkaline phosphatase histochemistry, immunohistochemistry, 1,1′-dioctadecyl-3,3,3′,3′-tetramethylindocarbocyanine perchlorate anterograde tracing of cortical axons, microscopy, image analysis and videotaping, two-texture and two-temperature preference assay, and number of mice analyzed and statistical analysis are described in *SI Materials and Methods*.

ACKNOWLEDGMENTS. The authors thank Drs. Andreas Hierholzer and Rolf Kemmler for sharing their *Cdx1-Cre* mouse line; Zixuan Pang for assistance with the thermal preference assay; Dr. Randy Reed for the gift of anti-Ebf1 antibodies; and Drs. Hao Chang, Amir Rattner, Hao Wu, and the two reviewers for helpful comments on the manuscript. This work was supported by the Howard Hughes Medical Institute, the Neurosurgery Pain Research Institute, and National Institute of Dental and Craniofacial Research Grant DEO22750.

1. Kolodkin AL, Tessier-Lavigne M (2011) Mechanisms and molecules of neuronal wiring: A primer. *Cold Spring Harb Perspect Biol* 3(6).

2. Bonanomi D, Pfaff SL (2010) Motor axon pathfinding. *Cold Spring Harb Perspect Biol* 2(3):a001735.

3. Feldheim DA, O'Leary DD (2010) Visual map development: Bidirectional signaling, bifunctional guidance molecules, and competition. *Cold Spring Harb Perspect Biol* 2(11):a001768.
4. Goodrich LV, Strutt D (2011) Principles of planar polarity in animal development. *Development* 138(10):1877–1892.
5. Wang Y, Zhang J, Mori S, Nathans J (2006) Axonal growth and guidance defects in Frizzled3 knock-out mice: A comparison of diffusion tensor magnetic resonance imaging, neurofilament staining, and genetically directed cell labeling. *J Neurosci* 26(2): 355–364.
6. Wang Y, Thekdi N, Smallwood PM, Macke JP, Nathans J (2002) Frizzled-3 is required for the development of major fiber tracts in the rostral CNS. *J Neurosci* 22(19): 8563–8573.
7. Tissir F, Bar I, Jossin Y, De Backer O, Goffinet AM (2005) Protocadherin Celsr3 is crucial in axonal tract development. *Nat Neurosci* 8(4):451–457.
8. Lyuksyutova AI, et al. (2003) Anterior-posterior guidance of commissural axons by Wnt-frizzled signaling. *Science* 302(5652):1984–1988.
9. Hua ZL, Smallwood PM, Nathans J (2013) Frizzled3 controls axonal development in distinct populations of cranial and spinal motor neurons. *eLife* 2:e01482.
10. Wu CS, et al. (2010) Requirement of cannabinoid CB(1) receptors in cortical pyramidal neurons for appropriate development of corticothalamic and thalamocortical projections. *Eur J Neurosci* 32(5):693–706.
11. Badea TC, et al. (2009) New mouse lines for the analysis of neuronal morphology using CreER(T)/loxP-directed sparse labeling. *PLoS ONE* 4(11):e7859.
12. Nakagawa Y, O'Leary DD (2003) Dynamic patterned expression of orphan nuclear receptor genes RORalpha and RORbeta in developing mouse forebrain. *Dev Neurosci* 25(2-4):234–244.
13. Chédotal A, Richards LJ (2010) Wiring the brain: The biology of neuronal guidance. *Cold Spring Harb Perspect Biol* 2(6):a001917.
14. NIH Neuroscience Blueprint Cre Driver Network (2009) *Cre Recombinase-Expressing Mice Generated for the NIH Neuroscience Blueprint Cre Driver Network. MGI Direct Data Submission* (Jackson Laboratory, Bar Harbor, ME).
15. Gorski JA, et al. (2002) Cortical excitatory neurons and glia, but not GABAergic neurons, are produced in the Emx1-expressing lineage. *J Neurosci* 22(15):6309–6314.
16. Stenman J, Toresson H, Campbell K (2003) Identification of two distinct progenitor populations in the lateral ganglionic eminence: implications for striatal and olfactory bulb neurogenesis. *J Neurosci* 23(1):167–174.
17. Hébert JM, McConnell SK (2000) Targeting of cre to the Foxg1 (BF-1) locus mediates loxP recombination in the telencephalon and other developing head structures. *Dev Biol* 222(2):296–306.
18. Zhou L, et al. (2008) Early forebrain wiring: Genetic dissection using conditional Celsr3 mutant mice. *Science* 320(5878):946–949.
19. López-Bendito G, et al. (2006) Tangential neuronal migration controls axon guidance: A role for neuregulin-1 in thalamocortical axon navigation. *Cell* 125(1):127–142.
20. Jacobowitz DM, Abbott LC (1998) *Chemoarchitectonic Atlas of the Developing Mouse Brain* (CRC, Boca Raton, FL).
21. Marquardt T, et al. (2001) Pax6 is required for the multipotent state of retinal progenitor cells. *Cell* 105(1):43–55.
22. Badea TC, Cahill H, Ecker J, Hattar S, Nathans J (2009) Distinct roles of transcription factors brn3a and brn3b in controlling the development, morphology, and function of retinal ganglion cells. *Neuron* 61(6):852–864.
23. Furuta Y, Lagutin O, Hogan BL, Oliver GC (2000) Retina- and ventral forebrain-specific Cre recombinase activity in transgenic mice. *Genesis* 26(2):130–132.
24. Fenstermaker AG, et al. (2010) Wnt/planar cell polarity signaling controls the anterior-posterior organization of monoaminergic axons in the brainstem. *J Neurosci* 30(47):16053–16064.
25. Zhuang X, Masson J, Gingrich JA, Rayport S, Hen R (2005) Targeted gene expression in dopamine and serotonin neurons of the mouse brain. *J Neurosci Methods* 143(1): 27–32.
26. Hierholzer A, Kemler R (2009) Cdx1:Cre allele for gene analysis in the extraembryonic ectoderm and the three germ layers of mice at mid-gastrulation. *Genesis* 47(3): 204–209.
27. Eng SR, et al. (2001) Defects in sensory axon growth precede neuronal death in Brn3a-deficient mice. *J Neurosci* 21(2):541–549.
28. Tissir F, et al. (2010) Lack of cadherins Celsr2 and Celsr3 impairs ependymal ciliogenesis, leading to fatal hydrocephalus. *Nat Neurosci* 13(6):700–707.
29. Wang Y, Nathans J (2007) Tissue/planar cell polarity in vertebrates: New insights and new questions. *Development* 134(4):647–658.
30. Gardner EP, Martin JH, Jessell TM (2000) The bodily senses. *Principles of Neural Science*, eds Kandel ER, Schwartz JH, Jessell TM (McGraw-Hill, New York), 4th Ed, pp 430–450.
31. Whelan PJ (1996) Control of locomotion in the decerebrate cat. *Prog Neurobiol* 49(5): 481–515.
32. Stuart DG, Hultborn H (2008) Thomas Graham Brown (1882–1965), Anders Lundberg (1920-), and the neural control of stepping. *Brain Res Brain Res Rev* 59(1):74–95.
33. Charbonneau V, Laramée ME, Boucher V, Bronchti G, Boire D (2012) Cortical and subcortical projections to primary visual cortex in anophthalmic, enucleated and sighted mice. *Eur J Neurosci* 36(7):2949–2963.
34. Klinge C, Eippert F, Röder B, Büchel C (2010) Corticocortical connections mediate primary visual cortex responses to auditory stimulation in the blind. *J Neurosci* 30(38): 12798–12805.
35. Watkins KE, et al. (2013) Early auditory processing in area V5/MT+ of the congenitally blind brain. *J Neurosci* 33(46):18242–18246.
36. Taniguchi H, et al. (2011) A resource of Cre driver lines for genetic targeting of GABAergic neurons in cerebral cortex. *Neuron* 71(6):995–1013.
37. Hayashi S, McMahon AP (2002) Efficient recombination in diverse tissues by a tamoxifen-inducible form of Cre: A tool for temporally regulated gene activation/inactivation in the mouse. *Dev Biol* 244(2):305–318.